EAI Endorsed Transactions
on Scalable Information Systems
Research Article EAI.EU

A Vehicle Target Tracking Method for Roadside Millimeter-Wave Radar

Hongcai Chen[1,2,*], Yu Cheng[1,2], Yaheng Ren[1,2] and Yaoxing Kang[1,2]

[1]Institute of Applied Mathematics, Hebei Academy of Sciences, Shijiazhuang 050081, China;
[2]Hebei Information Security Certification Technology Innovation Center, Shijiazhuang 050081, China

Abstract

INTRODUCTION: Roadside perception systems in intelligent transportation have stringent requirements for all-weather, high-precision, and real-time vehicle target tracking. However, there are inherent technical bottlenecks in such systems, including sparse millimeter-wave radar point clouds, severe noise interference, and the poor adaptability of traditional algorithms to distance-dependent density variations. OBJECTIVES: This study aims to propose a robust vehicle target tracking method based on roadside millimeter-wave radar to address the aforementioned technical bottlenecks and meet the stringent requirements of roadside perception systems for vehicle target tracking. METHODS: The research employs three key technical methods: Firstly, a point cloud distribution histogram is constructed to accurately localize the road area, and radar cross-section (RCS) characteristics are synergistically integrated with motion attributes to eliminate static clutter, multipath false plots, and electromagnetic noise. Secondly, a Distance-Zoned Multi-Frame DBSCAN (DZM-DBSCAN) clustering algorithm is proposed, which partitions the radar's effective detection range into near-distance and far-distance intervals based on the physical principle of point cloud density attenuation with increasing detection distance, dynamically optimizes clustering parameters (Eps, MinPts) for each interval using local density statistics from k-nearest neighbor (KNN) analysis, and suppresses single-frame isolated false clusters through inter-frame motion continuity constraints. Finally, a multi-target tracking framework is established by combining a dynamically threshold-adjusted Kalman Filter (KF) with multi-feature weighted Hungarian matching. RESULTS: The main results obtained in this paper are the following: Experimental validation on the public RadarData dataset shows that the DZM-DBSCAN algorithm achieves a Silhouette Coefficient (SC) of 0.8456, representing a 10.09% improvement over the traditional DBSCAN (0.7681), and a Davies-Bouldin Index (DBI) of 0.1936, which is 10.66% lower than that of the traditional DBSCAN (0.2167). This effectively resolves the long-distance target missing detection issue prevalent in conventional methods. Additionally, the proposed tracking method achieves an optimal balance between tracking accuracy and continuity, with an average single-frame processing time of only 1.08 ms, fully meeting the real-time requirements of roadside perception systems. CONCLUSION: The proposed robust vehicle target tracking method based on roadside millimeter-wave radar provides a reliable all-weather, high-precision, and real-time roadside vehicle perception solution for intelligent transportation systems. Thus, this work holds significant engineering application potential and theoretical value.

Keywords: millimeter-wave radar, point cloud clustering, DZM-DBSCAN, target tracking, Kalman filtering, hungarian algorithm.

Received on 01 September 2025, accepted on 25 November 2025, published on 01 July 2026

doi: 10.4108/eetsis.13848

*Corresponding author. Email: chenhongcai@heb-as.com

1. Introduction

With the rapid advancement of intelligent transportation systems (ITS), vehicle-infrastructure cooperation (V2I), and autonomous driving technologies have emerged as core pillars driving the transformation of modern transportation [1]. The roadside perception module, as the "perceptual nerve" of ITS, plays a critical role in enabling accurate, all-weather, and real-time positioning and tracking of vehicle targets, which is indispensable for ensuring traffic safety and optimizing traffic efficiency [2]. However, mainstream visual sensor-based perception solutions suffer from inherent limitations: they are highly susceptible to performance degradation or even failure under adverse weather conditions (e.g., rain, fog, heavy snow) and extreme lighting environments (e.g., strong glare, low illumination), while also struggling to meet the demanding requirements of centimeter-level positioning accuracy and millisecond-level processing latency [3].

In contrast, millimeter-wave radar has garnered significant attention as a key supplementary technology for roadside perception due to its unique advantages, including strong anti-interference capability, wide environmental adaptability, low cost, and direct measurement of target motion parameters (e.g., speed, distance) [4-5]. Nevertheless, in practical roadside application scenarios, millimeter-wave radar faces three prominent technical challenges: (1) Sparse point clouds, coupled with multipath effects, easily give rise to false plots, which severely degrade the quality of raw sensor data [6]; (2) In complex traffic scenarios involving multi-target trajectory crossing, occlusion, and high-speed movement, traditional tracking algorithms are prone to issues such as target identity switching, trajectory loss, and low matching robustness [7]; (3) Balancing high positioning accuracy with efficient computational performance remains a critical bottleneck to meet the real-time processing demands of roadside perception systems [8]. Therefore, conducting in-depth research on point cloud preprocessing, clustering, and multi-target tracking technologies tailored to the characteristics of millimeter-wave radar is of great significance for breaking through the current limitations of roadside perception and promoting the large-scale deployment of ITS.

Extensive research has been conducted in the academic community on millimeter-wave radar point cloud processing and multi-target tracking. In the field of point cloud clustering, the Density-Based Spatial Clustering of Applications with Noise (DBSCAN) algorithm [9-10] has been widely adopted due to its advantages of not requiring prior knowledge of the number of clusters and strong robustness to noise. However, the traditional DBSCAN algorithm has two critical drawbacks: it relies heavily on manually calibrated clustering parameters (Eps and MinPts), and these fixed parameters cannot adapt to the distance-dependent nonlinear density attenuation characteristics of millimeter-wave radar point clouds. This often leads to over-segmentation in near-distance regions (high point cloud density) and under-segmentation in far-distance regions (low point cloud density) [11].

To address the parameter adaptability issue, several improved DBSCAN variants have been proposed. For instance, Min et al. [12] proposed an improved DBSCAN algorithm based on density peaks to dynamically adjust Eps and MinPts; however, this method struggles to effectively identify density peaks in sparse, far-distance point cloud regions. Zhang et al. [13] introduced the WOA-DBSCAN algorithm, which utilizes the whale optimization algorithm to adaptively determine parameter ranges based on dataset distribution, but its optimization process increases computational complexity. Jin et al. [14] designed the ADBSCAN algorithm with a distance-adaptive clustering radius to enhance clustering quality, while El Yabroudi et al. [15] proposed an adaptive DBSCAN method based on field-of-view division and point cloud distance/density statistics, eliminating the need for manual parameter tuning. Despite these advancements, existing algorithms fail to fully account for the exponential decay of millimeter-wave radar point cloud density with distance, resulting in insufficient clustering accuracy and robustness across the entire detection range. Additionally, some methods suffer from high computational overhead, limiting their applicability in real-time systems.

In the realm of multi-target tracking, the traditional Kalman Filter (KF) combined with the Hungarian matching algorithm is widely used due to its computational efficiency and simplicity [16]. However, the linear motion assumption of the standard KF is incompatible with the nonlinear motion states of vehicles (e.g., acceleration, deceleration, lane changing), leading to inaccurate state estimation [17]. Moreover, the Hungarian matching algorithm typically constructs the cost matrix solely based on position features, which is prone to matching errors in scenarios involving target occlusion and trajectory crossing [18]. To mitigate these issues, Chang et al. [19] adopted the Extended Kalman Filter (EKF) to improve nonlinear state estimation, but this approach suffers from cumulative linearization errors. Nai et al. [20] proposed a multi-feature fusion-based target motion model estimation method, but it neglected the weight differences of different features under varying distance scenarios, resulting in inadequate matching robustness.

To address the aforementioned research gaps, this study proposes a comprehensive roadside millimeter-wave radar vehicle target tracking scheme that balances accuracy and real-time performance through three key technical innovations: point cloud preprocessing optimization, adaptive clustering parameter design, and multi-feature data association. The main contributions of this work are summarized as follows: (1) A three-level point cloud preprocessing pipeline ("road area localization → RCS screening → speed filtering") is designed, integrating spatial distribution characteristics and motion attributes to efficiently remove clutter and noise, thereby significantly improving the quality of point cloud data. (2) The DZM-DBSCAN clustering algorithm is proposed, which dynamically adjusts clustering parameters based on distance partitioning and eliminates multipath false clusters through inter-frame motion continuity constraints, effectively solving the problem

of unbalanced clustering accuracy in traditional algorithms across different density regions. (3) A multi-target tracking model is constructed by combining a dynamically threshold-adjusted KF with multi-feature weighted Hungarian matching, enabling accurate estimation of vehicle nonlinear motion states and stable tracking in complex traffic scenarios.

2. Point Cloud Clustering Method

2.1. Point Cloud Preprocessing

The millimeter-wave radar is mounted on a roadside bracket above the road, and a two-dimensional Cartesian coordinate system is established for data representation: the radar installation position is defined as the origin, the radar transmission direction (along the road) is the positive X-axis (longitudinal direction), and the direction perpendicular to the radar transmission plane and pointing to the left of the road is the positive Y-axis (lateral direction), forming an XOY plane coordinate system. The radar has a scanning angle of 120° and a detection distance range of 0-400 m, which can fully cover vehicle targets in multi-lane road scenarios, as illustrated in Figure 1.

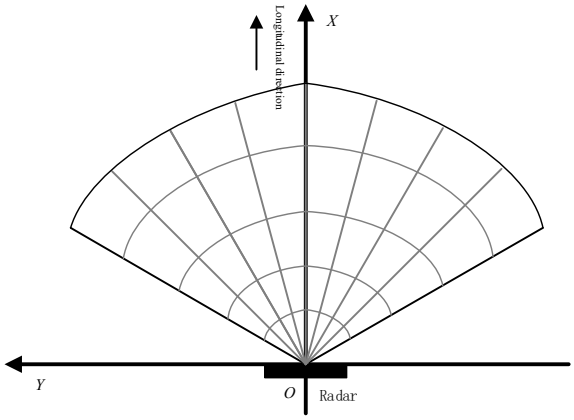

Figure 1. Schematic diagram of the radar coordinate system

2.1.1. Road Area Localization

In practical measurement scenarios, static objects such as buildings, green belts, and guardrails on both sides of the road generate a large amount of clutter, which exhibits a characteristic of edge concentration in the Y-axis (lateral) distribution. To accurately isolate the road area from the background clutter, this study proposes a road area localization method based on a point cloud Y-axis distribution histogram, with the specific steps as follows:

(1) Statistical analysis of Y-coordinate distribution: Count the Y-coordinate distribution of the original point cloud, set the statistical range to [-20 m, 20 m], and divide this interval into 20 equal-width bins to ensure sufficient resolution for distinguishing road regions.

(2) Histogram construction and feature extraction: Calculate the number of point clouds in each bin and plot the Y-axis point cloud distribution histogram. In the histogram, the peak regions correspond to lane positions (where vehicle point clouds are densely distributed), while the valley regions correspond to road edges (where clutter is sparse).

(3) Road area determination: Determine the Y-axis range [Y_min, Y_max] of the road area through histogram peak detection. For a standard 4-lane road (including lane markings, with a total width of approximately 15 m), combined with corrections for radar installation position deviations, the actual road area is typically constrained to [-8 m, 8 m]. Point clouds outside this range are classified as road edge clutter and directly removed.

Figure 2a presents the Y-axis coordinate distribution histogram of the point cloud, clearly demonstrating the dense distribution of point clouds within the road area. Road area localization can remove approximately 35%-45% of static edge clutter, with a computational complexity of only O(N) (where N is the number of point clouds), thus satisfying real-time requirements.

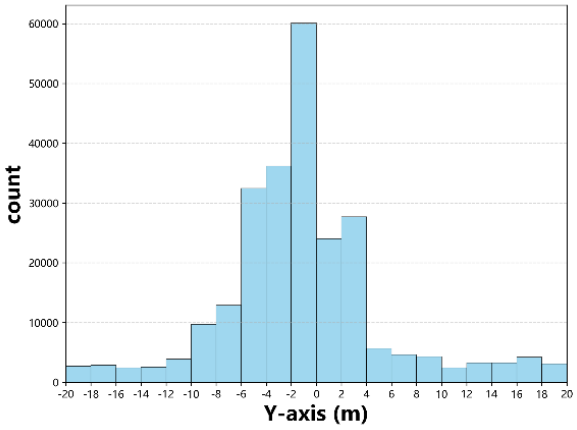

(a) Y-axis coordinate distribution histogram

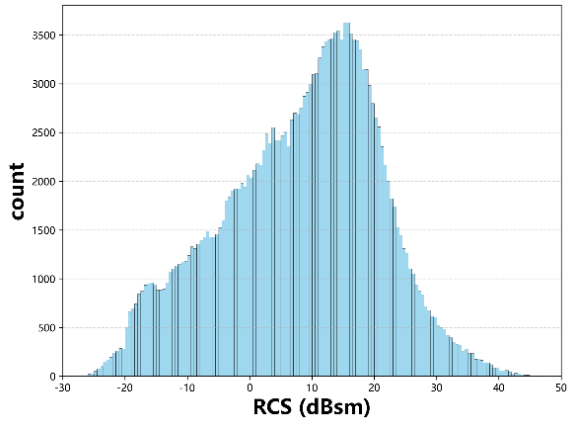

(b) RCS value distribution histogram

Figure 2. Statistical histograms of radar point cloud characteristics

2.1.2. Joint Screening Based on RCS and Velocity

Millimeter-wave radar point clouds are inevitably contaminated by atmospheric noise, multipath reflections, electromagnetic interference, and other factors, resulting in a large number of noise points. However, significant differences exist in RCS values and motion speeds between vehicle targets and clutter: (1) The RCS value of vehicle targets typically ranges from 5-20 dBsm (depending on vehicle type, orientation, and detection distance), while the RCS value of clutter (e.g., atmospheric noise, static objects) is mostly below 5 dBsm [4]; (2) The radial speed of static clutter (e.g., guardrails, street lamps) is 0 m/s, while the absolute radial speed of moving vehicles is generally greater than 2 m/s (excluding temporary parking scenarios) [5]. Based on these characteristics, a dual-threshold joint screening strategy is designed:

(1) RCS screening: Statistically analyze the RCS value distribution of point clouds within the road area (as shown in Figure 2b). It can be observed that the RCS values of most vehicle targets exceed 5 dBsm. Considering the RCS attenuation effect for long-distance vehicles, the RCS threshold is set to 3 dBsm, and point clouds with RCS values below this threshold are removed.

(2) Velocity screening: Set the lower velocity threshold v_{th1} =2 m/s to remove static point clouds with absolute radial velocity ≤ 2 m/s. Additionally, combined with the maximum radar detection velocity (usually ± 120 km/h), the upper velocity threshold v_{th2} =35 m/s (126 km/h) is set to eliminate abnormally high-velocity point clouds beyond this range.

Through the joint screening of RCS and velocity, approximately 25%-30% of the remaining clutter can be further removed, significantly improving the signal-to-noise ratio (SNR) of the point cloud data.

2.2. DZM-DBSCAN Clustering Algorithm

The traditional DBSCAN algorithm faces two core limitations in millimeter-wave radar point cloud processing: (1) Fixed clustering parameters (Eps, MinPts) cannot adapt to the nonlinear attenuation of point cloud density with detection distance, leading to over-segmentation in near-distance regions and under-segmentation in far-distance regions; (2) Single-frame independent clustering ignores the spatiotemporal continuity of targets, making it susceptible to generating false clusters or losing sparse targets due to clutter interference. To overcome these bottlenecks, this study proposes a Distance-Zoned Multi-Frame DBSCAN (DZM-DBSCAN) clustering algorithm, which integrates parameter adaptive optimization and spatiotemporal constraint enhancement to achieve accurate clustering of radar targets in complex scenarios.

2.2.1. Parameter Adaptability Based on Distance Partitioning

The spatial distribution density of millimeter-wave radar point clouds exhibits a significant negative correlation with the detection distance r [17], which is essentially attributed to the spherical diffusion effect of radar transmitted signals and the distance dependence of the target RCS. Specifically, as the detection distance increases, the number of effective echo points per unit space decreases nonlinearly, and the dispersion of point clouds for far-distance targets increases significantly. To quantify this characteristic, actual road measurements were conducted to collect point clouds covering the 0-400 m effective detection range, and the point cloud number density in different distance intervals was statistically analyzed to generate a distribution histogram (Figure 3).

As shown in Figure 3, the point cloud density exhibits a distinct segmentation characteristic at 200 m: the point cloud density within 200 m is concentrated above 600 units, while the density beyond 200 m drops sharply to approximately 200 units. Based on this distribution law, the radar's 0-400 m effective detection range is partitioned into a near-distance interval ($r \in [0, 200$ m]) and a far-distance interval ($r \in [200$ m, 400 m]). For each interval, a differentiated parameter adaptive mechanism is designed to dynamically match clustering parameters with point cloud characteristics, clutter distribution, and target density:

(1) Parameter adaptive design for the near-distance interval ($r \in [0, 200$ m])

The near-distance interval is characterized by high point cloud density, dense targets, and severe clutter interference. A single vehicle target typically generates 2-10 detection points, and the point clouds exhibit strong aggregation but are easily confused with adjacent target point clouds. To balance clustering integrity and anti-interference capability, a two-factor parameter adaptive strategy combining KNN density statistics and RCS semantic assistance is adopted:

Adaptive Eps parameter calculation: The KNN algorithm with K = 5 is used to count the local point cloud density, and the average distance of 5 near neighbors is calculated as the local density metric for each point. The median of this average distance across all points is selected as the baseline Eps value for this interval, ensuring coverage of the local neighborhood range for more than 50% of the target points.

Baseline MinPts parameter setting: Considering that most near-distance clutter points are distributed as isolated points or small clusters, the baseline $MinPts_1$=3 is set to ensure that the clustering clusters have a sufficient spatial aggregation, thereby avoiding misclassifying clutter as targets.

RCS semantic adjustment mechanism: RCS, as a direct reflection of target physical properties, can effectively distinguish between vehicle types (e.g., trucks, cars) and non-vehicle targets. By statistically analyzing the RCS distribution characteristics of different target types, the following parameter adjustment rules are established:

$$\begin{cases} Eps = 2.0\text{ m}, MinPts = 2, \text{ if RCS} < 20\text{ dBsm}, \\ Eps = 2.5\text{ m}, MinPts = 2, \text{ if } 20\text{ dBsm} \le \text{RCS} \le 25\text{ dBsm}, \\ Eps = 3.0\text{ m}, MinPts = 3, \text{ if RCS} > 25\text{ dBsm}. \end{cases}$$

Here, RCS > 25 dBsm corresponds to large vehicles (e.g., trucks), 20 dBsm ≤ RCS ≤ 25 dBsm corresponds to medium-sized vehicles (e.g., cars), and RCS < 20 dBsm

corresponds to small traffic targets or long-distance vehicles. By fusing target semantic information, this mechanism upgrades the parameters from global adaptability to target-level adaptability, effectively resolving clustering segmentation issues in near-distance multi-target mixed scenarios.

(2) Parameter adaptive design for the far-distance interval ($r \in (200\text{ m}, 400\text{ m}]$)

The far-distance interval is characterized by low point cloud density, weak clutter interference, and sparse target point clouds (a single vehicle target typically generates only 1-3 detection points). Traditional fixed parameters often misclassify real targets as noise or form fragmented clusters. To address this, a strategy combining low-density adaptive parameters and speed consistency verification is adopted:

Baseline parameter adaptation: Considering the large dispersion of long-distance point clouds, the KNN algorithm with $K = 3$ is used to calculate the Eps value; at the same time, $MinPts_2 = 2$ is set to lower the threshold of forming clusters, avoiding misjudging real long-distance targets with only 1-2 points as noise.

False cluster removal mechanism: Although far-distance scenarios have less clutter, isolated point clusters may still be formed by radar noise or ground reflections. Leveraging the motion continuity of vehicle targets (i.e., the radial speeds of point clouds belonging to the same target should be highly consistent, while the speed distribution of noise point clusters is disorderly), a radial speed standard deviation threshold of 1 m/s, it is classified as a false cluster (noise or interference) and removed; otherwise, it is retained as a real target cluster. This mechanism compensates for the lack of spatial aggregation in long-distance sparse point clouds, enabling effective identification of false clusters.

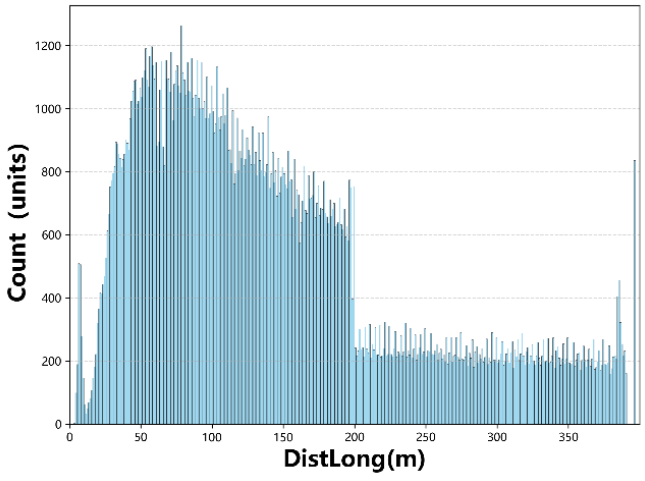

Figure 3. Distribution histogram of radar point cloud density as a function of detection distance

2.2.2. False Cluster Removal Strategy Based on Multi-Frame Fusion

Multipath effects can introduce isolated false plots in single-frame point clouds, which lack motion continuity across consecutive frames. These false plots can be effectively removed through inter-frame motion consistency constraints, with the specific steps as follows:

Step 1: Inter-frame point cloud association

Let the current frame be the k-th frame and the previous frame be the $(k-1)$-th frame. For each vehicle cluster obtained by DZM-DBSCAN clustering of the $(k-1)$-th frame, calculate its center point coordinates (x_{k-1}, y_{k-1}) and average radial speed v_{k-1}. Based on the uniform motion model, the center point coordinates of the vehicle cluster in the k-th frame are predicted as:

$$(\hat{x}_k, \hat{y}_k) = (x_{k-1} + v_{k-1} \cdot \Delta t, y_{k-1})$$

where Δt is the inter-frame time interval (determined by the radar sampling frequency).

Step 2: False plot removal

Calculate the Euclidean distance d between the center point (x_k, y_k) of each candidate cluster in the k-th frame and all predicted center points of the $(k-1)$-th frame. Set the matching threshold Eps_{match} = 5 m (determined based on radar positioning accuracy and vehicle motion speed). If there exists a predicted center point such that $d < Eps_{match}$, the candidate cluster is judged as a real vehicle cluster. If the distance between the candidate cluster and all predicted center points exceeds Eps_{match}, for 3 consecutive frames, it is classified as a false cluster and removed.

Step 3: Clustering result smoothing

For real vehicle clusters, the sliding average of their center point coordinates is calculated (using the average of the center point coordinates of the current frame and the previous two frames) to achieve temporal smoothing of the point clouds and reduce noise interference:

$$\begin{cases} \bar{x}_k = (x_k + x_{k-1} + x_{k-2})/3 \\ \bar{y}_k = (y_k + y_{k-1} + y_{k-2})/3 \end{cases}$$

2.2.3. DZM-DBSCAN Algorithm Flow

The specific execution flow of the DZM-DBSCAN algorithm is as follows:

Step 1: Input preprocessed point cloud data of the k-th frame, clustering results of the $(k-1)$-th frame (including vehicle cluster center point coordinates and average speed).

Step 2: Distance partitioning: Divide the point cloud into the near-distance region R_1 (0-200 m) and the far-distance region R_2 (200-400 m) based on X-axis coordinates (detection distance).

Step 3: Adaptive parameter calculation: For R_1 use the K-NN algorithm with K = 5 to calculate Eps_1, adjust parameters according to RCS values, and set $MinPts_1$; for R_2, use the K-NN algorithm with K=3 to calculate Eps_2, and set $MinPts_2$=2;

Step 4 Partitioned clustering: Perform DBSCAN clustering on R_1 and R_2 separately to obtain candidate clusters.
Step 5 Multi-frame fusion: Predict the vehicle cluster center points of the k -th frame based on the clustering results of the ($k-1$)-th frame, calculate the Euclidean distance between candidate clusters and predicted center points, remove false clusters, and retain real vehicle clusters.
Step 6 Smoothing processing: Calculate the sliding average of the center points of real vehicle clusters.
Step 7: Output the clustering results of vehicle targets in the k -th frame.

2.3. Vehicle Target Tracking Method

The core of vehicle target tracking lies in the closed-loop process of "prediction → observation → matching → update"[21]. This study improves the state estimation capability of the KF and optimizes the cost function of the Hungarian matching algorithm to enhance tracking performance in complex traffic scenarios.

2.3.1. Improved Kalman Filter

A dynamically threshold-adjusted Kalman filter is designed to achieve accurate estimation of target motion states and effective detection of motion mutations.
(a) State Model:
In roadside scenarios, vehicles can be approximately modeled as moving at a constant speed in a straight line within a short time window. A constant velocity motion model is adopted to balance tracking accuracy and computational efficiency. The state vector is defined as:

$$X=[x,y,v_x,v_r]^T \tag{1}$$

where x and y are the longitudinal (X-axis) and lateral (Y-axis) position coordinates of the point cloud target, respectively; v_x and v_y are the longitudinal and lateral velocities, respectively.
The state transition equation, which describes the vehicle motion characteristics, is given by:

$$X_k=F\cdot X_{k-1}+W_{k-1} \tag{2}$$

where F is the state transition matrix, and W_{k-1} is the process noise, which follows a Gaussian distribution with a mean of 0 and a covariance matrix of Q . Through offline experiments, Q is calibrated as a diagonal matrix with diagonal elements [0.0001, 0.0001, 0.0001, 0.0001].
(b) Observation Model
The observation equation is defined as:

$$Z_k=H\cdot X_k+V_k \tag{3}$$

where Z_k is the observation vector obtained from clustering, H is the observation matrix, and V_k is the observation noise, which follows a Gaussian distribution with a mean of 0 and a covariance matrix of R .
(c) Dynamic Noise Covariance Adjustment
To address distance-related measurement errors, the observation noise covariance matrix R is dynamically optimized:
When the target distance $Dist$ < 200 m, the basic covariance matrix $base_R$ is adopted, with diagonal elements [1, 1, 0.01, 0.01];
When $Dist$ ⩾ 200 m, a scaling factor $Scale$ = 1 + ($Dist$ - 200)/400 is introduced to adjust the weight of R , thereby reducing the impact of long-distance measurement errors on state estimation. The adjusted covariance matrix is $R=base_R\times Scale$.
(d) State Prediction
Based on the state estimation and covariance matrix of the ($k-1$)-th frame, the predicted state and predicted covariance of the k -th frame are calculated as:

$$\hat{X}_{k|k-1}=F\cdot\hat{X}_{k-1|k-1} \tag{4}$$

$$\hat{P}_{k|k-1}=F\cdot\hat{P}_{k-1|k-1}\cdot F^{\mathrm{T}}+Q \tag{5}$$

Where $\hat{X}_{k-1|k-1}$ is the state estimation value of the ($k-1$)-th frame, and $\hat{P}_{k-1|k-1}$ is the state estimation covariance matrix of the ($k-1$)-th frame.
(e) Observation Update
The Kalman gain is calculated, and the state estimation and covariance matrix are updated by combining the current frame observation value:

$$K_k=\hat{P}_{k|k-1}\cdot H^{\mathrm{T}}\cdot\left(H\cdot\hat{P}_{k|k-1}\cdot H^{\mathrm{T}}+R\right)^{-1} \tag{6}$$

$$\hat{X}_{k|k}=\hat{X}_{k|k-1}+K_k\cdot\left(Z_k-H\cdot\hat{X}_{k|k-1}\right) \tag{7}$$

$$P_{k|k}=(I-K_k\cdot H)\cdot P_{k|k-1} \tag{8}$$

Where I is the identity matrix.

2.3.2. Multi-Feature Weighted Hungarian Matching

To improve the robustness of data association in complex scenarios (e.g., target occlusion, trajectory crossing), the association cost matrix is constructed by fusing the point cloud position and velocity dynamic features, with the specific steps as follows:
(a) Feature Normalization
Position error and velocity errors are normalized to eliminate the influence of dimension differences. The normalization formula is:

$$e^{'}=(e-e_{\min})/(e_{\max}-e_{\min}) \tag{9}$$

where e is the original error, $e_{\min}$ and $e_{\max}$ are the minimum and maximum values of the feature error in the current frame, respectively.
(b) Cost Matrix construction
Position and velocity features are fused, and feature weights are optimized through grid search to adapt to different distance scenarios. The cost function is defined as:

$$c_{ij}=\omega_1\cdot\sqrt{\Delta x_{ij}^{'2}+\Delta y_{ij}^{'2}}+\omega_1\cdot\Delta v_{ij}^{'} \tag{10}$$

Where c_{ij} is the association cost between the i -th predicted trajectory and the j -th observation result; ω_1 and ω_2 are feature weights optimized via grid search (in short-range scenarios, ω_1 =0.6, ω_2 =0.4, in long-range scenarios, ω_1

=0.5, ω_2 =0.5,); $\Delta x_{ij}^{'}$, $\Delta y_{ij}^{'}$, and $\Delta v_{ij}^{'}$ are the normalized longitudinal position errors, lateral position error, and velocity error, respectively.

(c) Matching and Tracking Management:

The cost matrix is input into the Hungarian algorithm to solve for the optimal matching. For unmatched observations, a new tracker is initialized; for predicted trajectories that remain unmatched for 5 consecutive frames, the target is judged to have left the detection area, and the tracker is terminated.

The overall flowchart of the vehicle target tracking model is shown in Figure 4.

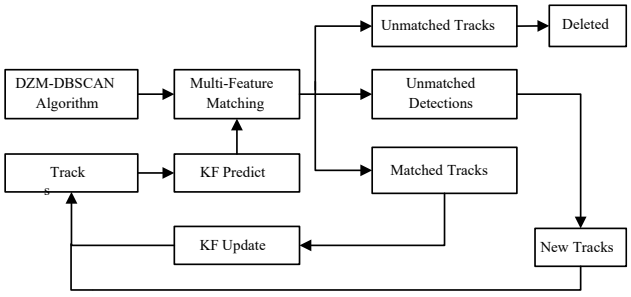

Figure 4. Overall flowchart of the proposed vehicle target tracking method

3. Experiments

3.1. Experimental Datasets and Environment

To comprehensively verify the effectiveness and superiority of the proposed roadside millimeter-wave radar vehicle target tracking method, a series of experiments is designed to evaluate performance from multiple dimensions, including point cloud clustering quality, target tracking accuracy, and real-time processing efficiency.

Data Description: The public RadarData dataset [22] was used for experimental verification. This dataset was collected by Pazhou Laboratory (Whampoa) and contains high-precision millimeter-wave radar point cloud data from a real-road scenario. The key parameters of the millimeter-wave radar are as follows: 4 transmitters (TX) and 2 × 6 receivers (RX), data output interval of 70-80 ms, distance accuracy < 0.4 m, velocity accuracy < 0.0277m/s, scanning angle of 120 °, and detection distance of 0-400 m. The test road is a one-way four-lane road (3.6 m per lane) with a speed limit of 60 km/h, covering various traffic scenarios such as normal driving, lane changing, and target occlusion.

Experiment environment:

(1) Hardware: Intel Core i7-12700K CPU (3.6 GHz), 32GB DDR4 memory;

(2) Software: Windows 11 operating system, Python 3.8 programming language, with implementations based on NumPy, SciPy, Scikit-learn, and Pandas libraries.

3.2. Point Cloud Target Clustering Analysis

To verify the superiority of the DZM-DBSCAN clustering algorithm, the traditional DBSCAN [9] and ADBSCAN [14] algorithms were selected as baseline methods for comparison. Since the RadarData dataset lacks ground-truth target labels, internal clustering evaluation metrics — Silhouette Coefficient (SC) and Davies-Bouldin Index (DBI)) — were used to assess clustering quality. The SC range from [-1, 1], with values closer to 1 indicating more reasonable clustering (i.e., higher intra-cluster compactness and inter-cluster separation, and smaller values indicating better clustering performance.

Table 1 presents the quantitative evaluation results of the three clustering algorithms. It can be observed that the DZM-DBSCAN algorithm achieves an average SC of 0.8456, which is 10.09% higher than that of the traditional DBSCAN (0.7681) and 4.36% higher than that of ADBSCAN (0.8103). Meanwhile, the DBI of DZM-DBSCAN is 0.1936, which is 10.66% lower than that of the traditional DBSCAN (0.2167) and 6.02% lower than that of ADBSCAN (0.2060). The traditional DBSCAN exhibits a relatively high DBI value of 0.2167, reflecting its inherent limitations of insufficient intra-cluster compactness and poor inter-cluster separation, particularly in handling distance-dependent density variations.

Table 1. Clustering performance evaluation metrics of different algorithms

Clustering Algorithm	Silhouette Coefficient (SC)	Davies-Bouldin Index(DBI)
DBSCAN [9]	0.7681	0.2167
ADBSCAN [14]	0.8103	0.2060
DZM-DBSCAN	0.8456	0.1936

To intuitively demonstrate the clustering effect, representative frames from the dataset were selected for visualization comparison, as shown in Figure 5. Figure 5a,b presents the clustering results of the traditional DBSCAN algorithm. The traditional DBSCAN can only correctly cluster near-distance targets, while far-distance sparse point clouds (200-400 m) are misclassified as noise. This is because the fixed parameters of the traditional DBSCAN cannot adapt to the low density of far-distance point clouds, leading to under-segmentation. In contrast, Figure 5c,d shows the clustering results of the proposed DZM-DBSCAN algorithm. By leveraging distance-zoned adaptive parameters and multi-frame fusion constraints, the DZM-DBSCAN algorithm effectively identifies and clusters both near-distance and far-distance targets, with clear clustering boundaries and no obvious over-segmentation or under-segmentation. This confirms the superior clustering performance of the DZM-DBSCAN algorithm across the entire detection range.

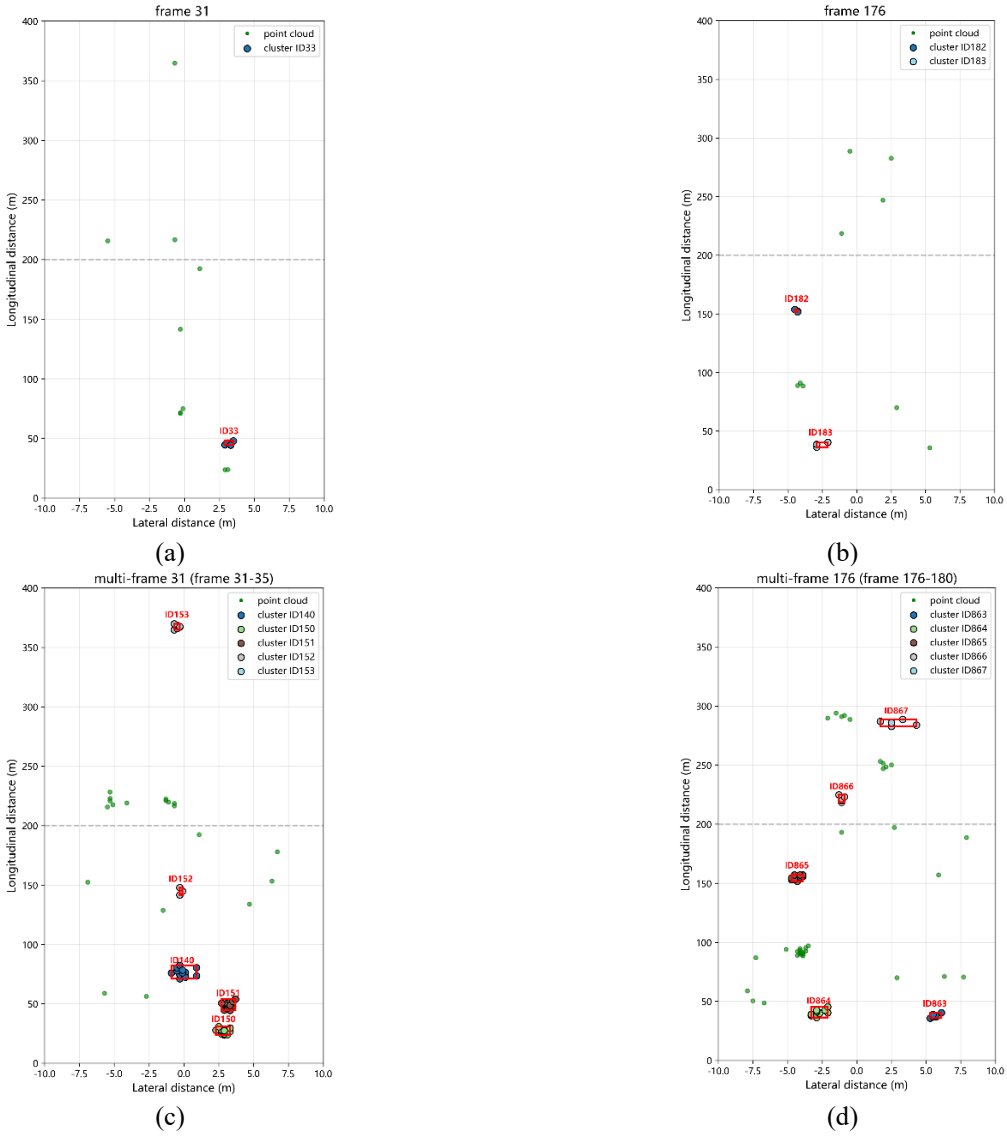

Figure 5. Visual comparison of point cloud clustering results: (a,b) Traditional DBSCAN (frames 31 and 176); (c,d) Proposed DZM-DBSCAN (frames 31-35 and 176-180)

3.3. Analysis of Point Cloud Target Tracking Performance

To evaluate the tracking performance of the proposed method, three comparison algorithms were selected: (1) Traditional KF + Hungarian matching (KF + Hungarian) [16]; (2) Improved KF + Hungarian matching (Improved KF + Hungarian); (3) Proposed dynamically threshold-adjusted KF + multi-feature weighted Hungarian matching (Proposed Method).

The visualization results of target tracking are shown in Figure 6. Figure 6a presents the tracking results of the traditional KF + Hungarian matching method in scenarios involving high-speed target motion and trajectory crossing. It can be observed that this method suffers from trajectory interruptions and identity switching for individual targets, primarily due to the linear motion assumption of the traditional KF and the single-position-feature-based matching strategy. Figure 6b shows the tracking results of the Improved KF + Hungarian matching method. The dynamic threshold adjustment of the KF effectively mitigates trajectory interruptions, but target identity switching still occurs in complex scenarios, as the matching strategy remains reliant on a single feature. In contrast, Figure 6c demonstrates the tracking results of the proposed method. By integrating the dynamically adjusted KF with multi-feature weighted Hungarian matching, the proposed method achieves stable target tracking without trajectory interruptions or identity switching, even in complex scenarios involving high-speed motion and trajectory crossing. This confirms the superior robustness and accuracy of the proposed tracking framework.

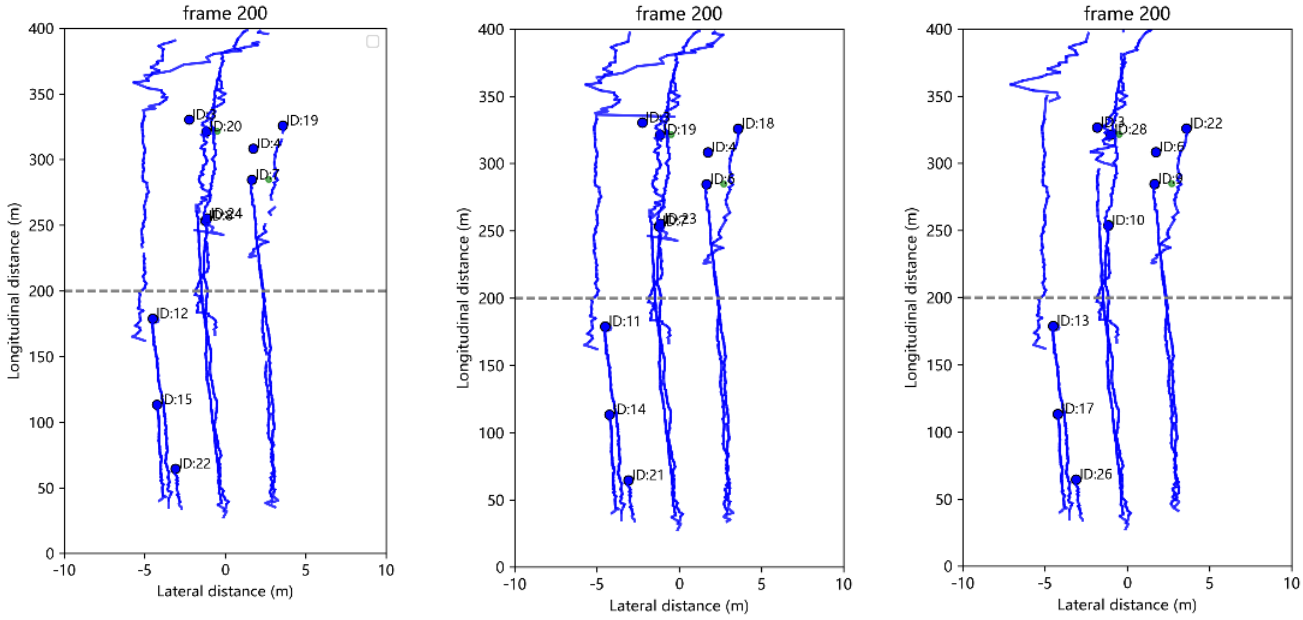

(a) (b) (c)

Figure 6. Visual comparison of target tracking results: (a) Traditional KF + Hungarian; (b) Improved KF + Hungarian; (c) Proposed method (frame 200)

3.4. Real-Time Performance Analysis

The real-time performance of different algorithms was evaluated on the RadarData dataset, which contains a total of 2.83 million millimeter-wave radar point cloud data points. After merging data with the same timestamp into a single frame, the dataset consists of 15,538 frames. The total processing time and average single-frame processing time of each algorithm are summarized in Table 2.

Table 2. Real-time performance comparison of different algorithms

Algorithm	Total Processing Time /s	Average Single-Frame Process/ms
DBSCAN+KF+ Hungarian	13.2	0.85
DZM-BSCAN+KF+ Hungarian	15.8	1.02
DZM-DBSCAN+ improved KF+ Hungarian	16.2	1.04
Proposed Method	16.8	1.08

As shown in Table 2, the total processing time of the proposed method (including preprocessing, clustering, and tracking) is 16.8 s, corresponding to an average single-frame processing time of 1.08 ms, which fully meets the millisecond-level real-time requirements of roadside perception systems. The traditional method (DBSCAN + KF + Hungarian) exhibits the shortest total processing time (13.2 s), but its clustering and tracking performance are significantly inferior. The DZM-DBSCAN clustering module increases the total processing time by 2.6 s compared to the traditional DBSCAN, primarily due to the additional distance partitioning, adaptive parameter calculation, and multi-frame fusion steps. However, this overhead is negligible and within the acceptable range for real-time applications. The improved KF + multi-feature weighted Hungarian matching module adds 0.6 s of processing time compared to the traditional KF + Hungarian method, which is attributed to the dynamic noise covariance adjustment and multi-feature normalization processes. Overall, the proposed method achieves an optimal balance between tracking accuracy and real-time performance, making it suitable for practical roadside perception applications.

4. Conclusion

Aiming at the limitations of visual sensors in all-weather vehicle target tracking and the technical bottlenecks of millimeter-wave radar in roadside perception, this study proposes a high-precision and real-time vehicle target tracking method based on roadside millimeter-wave radar. Through a multi-level technical architecture integrating point cloud preprocessing, improved DBSCAN clustering, and optimized KF tracking, the proposed method achieves accurate identification and stable tracking of vehicle targets in complex traffic scenarios. The main research conclusions are as follows:

(1) A three-level point cloud preprocessing pipeline ("road area localization → RCS screening → speed filtering") is

proposed. By synergistically integrating spatial distribution characteristics and motion attributes, this pipeline effectively removes static clutter and dynamic noise, significantly improving the quality of point cloud data and laying a solid foundation for subsequent clustering and tracking.

(2) The DZM-DBSCAN clustering algorithm is developed. Based on distance-zoned adaptive parameter adjustment and inter-frame motion continuity constraints, this algorithm solves the problem of unbalanced clustering accuracy of traditional DBSCAN in different density point cloud regions. Experimental results show that the DZM-DBSCAN algorithm achieves a Silhouette Coefficient of 0.8456 and a Davies-Bouldin Index of 0.1936, outperforming the traditional DBSCAN and ADBSCAN algorithms.

(3) A dynamically threshold-adjusted Kalman Filter is constructed to enhance the adaptability of state estimation to target motion variations, and a multi-feature weighted Hungarian matching cost function is designed to improve the robustness of data association in complex scenarios. The proposed tracking method achieves an average single-frame processing time of 1.08 ms, meeting the real-time requirements of roadside perception systems while ensuring high tracking accuracy and continuity.

Despite the promising results, this study has certain limitations: millimeter-wave radar point clouds lack detailed vehicle appearance feature information, making it difficult to achieve accurate vehicle type classification. In future work, we plan to construct a "radar + vision" multi-sensor fusion perception system, combining the advantages of radar in motion parameter measurement and vision in appearance feature recognition to enrich the diversity of target information. Additionally, we will further explore advanced multi-sensor fusion algorithms to improve the robustness and generalization ability of roadside perception systems, providing a more comprehensive and reliable solution for intelligent transportation systems.

Author Contribution

Conceptualization, H.C. and Y.C.; methodology, H.C.; software, H.C and Y.K.; validation, H.C., Y.R., and Y.K.; formal analysis, H.C.; data curation, Y.R.; writing—original draft preparation, H.C.; writing—review and editing, Y.C.; visualization, H.C. and Y. K.; project administration, Y.C.; funding acquisition, Y.C. All authors have read and agreed to the published version of the manuscript.

Funding

This research was funded by the Science and Technology Plan Project of Hebei Academy of Sciences (No. 25601), the Hebei Provincial Innovation Capacity Enhancement Program (No.24460802D).

Data Availability

The datasets used in this study are publicly available. The RadarData dataset can be accessed at https://iacc.pazhoulab-huangpu.com/contestdetail?id=64af500a4a0ed647faca6230&-award=1,000,000.

Acknowledgment

This work was financially supported by the Science and Technology Plan Project of Hebei Academy of Sciences (No. 25601) entitled “Research on Vehicle Trajectory Tracking Technology Based on Multi-Source Data Fusion. The authors would like to express their sincere gratitude to the project management team for their valuable guidance and support throughout the research process. They also thank Pazhou Laboratory (Whampoa) for providing the RadarData dataset for experimental validation.

Competing Interest

The authors have no relevant financial or non-financial interests to disclose.

Ethical Approval

Not applicable.

References

[1] Yi X, Rui Y, Ran B, et al. Vehicle–Infrastructure Cooperative Sensing: Progress and Prospect[J]. Strategic Study of Chinese Academy of Engineering, 2024, 26(1): 178-189.

[2] Liu L, Lu S, Zhong R, et al. Computing systems for autonomous driving: State of the art and challenges[J]. IEEE Internet of Things Journal, 2020, 8(8): 6469-6486.

[3] Zhang X, Wang H, Dong H. A Survey of Deep Learning-Driven 3D Object Detection: Sensor Modalities, Technical Architectures, and Applications[J]. Sensors, 2025, 25(12): 3668.

[4] Wang S, Mei L, Liu R, et al. Multi-modal fusion sensing: A comprehensive review of millimeter-wave radar and its integration with other modalities[J]. IEEE Communications Surveys & Tutorials, 2024, 27(1): 322-352.

[5] Yan B, Roberts I P. Advancements in Millimeter-Wave Radar Technologies for Automotive Systems: A Signal Processing Perspective[J]. Electronics, 2025, 14(7): 1436.

[6] LIU Zhihao, SHANG Yuanyuan, LI Timing, et al. Robust multi-drone multi-target tracking to resolve target occlusion: A benchmark[J]. IEEE Transactions on Multimedia, 2023, 25: 1462-1476.

[7] KULKARNI O, BURHANPURWALA A. A survey of advancements in DBSCAN clustering algorithms for big data[C]//2024 3rd International Conference on Power Electronics and IoT Applications in Renewable Energy and Its Control (PARC). Mathura, India. IEEE, 2024: 106-111.

[8] SINGH H V, GIRDHAR A, DAHIYA S. A literature survey based on DBSCAN algorithms[C]//2022 6th International Conference on Intelligent Computing and Control Systems (ICICCS). Madurai, India. IEEE, 2022: 751-758.

[9] Ester M, Kriegel H P, Sander J, et al. A density-based algorithm for discovering clusters in large spatial databases

with noise[C]//Proceedings of the 2nd International Conference on Knowledge Discovery and Data Mining. Portland, USA: AAAI Press, 1996: 226-231.
[10] Sander J, Ester M, Kriegel H P, et al. Density-based clustering in spatial databases: The algorithm GDBSCAN and its applications[J]. Data Mining and Knowledge Discovery, 1998, 2(2): 169-194.
[11] Zhu L, Liu G, Hui G, et al. An Unmanned Vehicle Inspection System for Airport Runways[C]//2022 12th International Conference on CYBER Technology in Automation, Control, and Intelligent Systems (CYBER). IEEE, 2022: 1171-1176.
[12] MIN Xiangqiang, HUANG Yi, SHENG Yehua. Automatic determination of clustering centers for “clustering by fast search and find of density peaks”[J]. Mathematical Problems in Engineering, 2020, 2020: 4724150.
[13] Zhang X, Zhou S. WOA-DBSCAN: application of whale optimization algorithm in DBSCAN parameter adaption[J]. IEEE Access, 2023, 11: 91861-91878.
[14] Jin X, Yang H, He X, et al. Robust LiDAR-based vehicle detection for on-road autonomous driving[J]. Remote Sensing, 2023, 15(12): 3160.
[15] El Yabroudi M, Awedat K, Chabaan R C, et al. Adaptive DBSCAN LiDAR point cloud clustering for autonomous driving applications[C]//2022 IEEE International Conference on Electro Information Technology (eIT). IEEE, 2022: 221-224.
[16] Mei F, Zhou H, Su J, et al. A Kalman filter-Hungarian algorithm with a postprocessor for tracking aeolian saltating particle in high-speed video[J]. Earth Surface Processes and Landforms, 2024, 49(15): 5086-5097.
[17] Sengupta A, Cheng L, Cao S. Robust multiobject tracking using mmwave radar-camera sensor fusion[J]. IEEE Sensors Letters, 2022, 6(10): 1-4.
[18] Szűcs G, Borsodi R, Papp D. Multi-camera trajectory matching based on hierarchical clustering and constraints[J]. Multimedia Tools and Applications, 2024, 83(15): 44879-44902.
[19] Chang S Y, Wu H C, Kao Y C. Tensor extended Kalman filter and its application to traffic prediction[J]. IEEE Transactions on Intelligent Transportation Systems, 2023, 24(12): 13813-13829.
[20] Nai K, Li Z, Wang H. Dynamic feature fusion with spatial-temporal context for robust object tracking[J]. Pattern Recognition, 2022, 130: 108775.
[21] Yuan X, Wang S, Xie Y, et al. Object-Based Semantic Fusion Algorithm of Lidar and Camera via Inverse Projection[J]. IEEE Transactions on Instrumentation and Measurement, 2025.
[22] RadarData. Calibration and target tracking of roadside millimeter-wave radar [EB/OL]. Guangzhou: Pazhou Laboratory (Whampoa), China, 2023[2025-09-01]. https://iacc.pazhoulabhuangpu.com/contestdetail?-id=64af500-a4a0ed647faca6230&- award=1,000,000. unpublished